ACS APPLIED MATERIALS & INTERFACES

Research Article

www.acsami.org

Green Synthesis of Anisotropic Gold Nanoparticles for Photothermal Therapy of Cancer

Sajid Fazal, Aswathy Jayasree, Sisini Sasidharan, Manzoor Koyakutty, Shantikumar V. Nair, and Deepthy Menon*

Amrita Centre for Nanoscience and Molecular Medicine, Amrita Institute of Medical Science and Research Centre, Amrita Vishwa Vidyapeetham University, Edappally, Kochi-682041, Kerala India

Supporting Information

ABSTRACT: Nanoparticles of varying composition, size, shape, and architecture have been explored for use as photothermal agents in the field of cancer nanomedicine. Among them, gold nanoparticles provide a simple platform for thermal ablation owing to its biocompatibility in vivo. However, the synthesis of such gold nanoparticles exhibiting suitable properties for photothermal activity involves cumbersome routes using toxic chemicals as capping agents, which can cause concerns in vivo. Herein, gold nanoparticles, synthesized using green chemistry routes possessing near-infrared (NIR) absorbance facilitating photothermal therapy, would be a viable alternative. In this study, anisotropic gold nanoparticles were synthesized using an aqueous route with cocoa extract which served both as a reducing and stabilizing agent. The as-prepared gold nanoparticles were subjected to density gradient centrifugation to maximize its NIR absorption in the wavelength range of 800−1000 nm. The particles also showed good biocompatibility when tested in vitro using A431, MDA-MB231, L929, and NIH-3T3 cell lines up to concentrations of 200 μg/mL. Cell death induced in epidermoid carcinoma A431 cells upon irradiation with a femtosecond laser at 800 nm at a low power density of 6 W/cm^2 proved the suitability of green synthesized NIR absorbing anisotropic gold nanoparticles for photothermal ablation of cancer cells. These gold nanoparticles also showed good X-ray contrast when tested using computed tomography (CT), proving their feasibility for use as a contrast agent as well. This is the first report on green synthesized anisotropic and cytocompatible gold nanoparticles without any capping agents and their suitability for photothermal therapy.

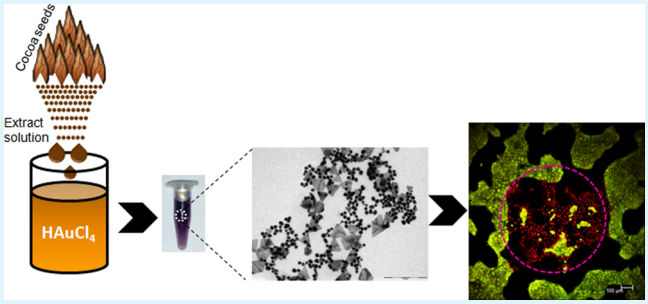

KEYWORDS: *gold nanoparticles, green route, photothermal therapy, anisotropic nanoparticles, cocoa, cancer*

INTRODUCTION

With the advent of nanotechnology in life sciences, the field of cancer therapy and diagnosis has expanded through the inclusion of various arsenals in the form of polymeric nanodrug delivery vehicles,[1] iron-oxide nanoparticles for magnetic hyperthermia,[2] metallic nanoparticles for photothermal[3] and radiothermal therapy,[4−7] quantum dots for fluorescent imaging diagnosis,[8] Magnetic resonance imaging and computed tomography contrast agents,[9−11] etc. In the past decade, there have been a number of significant contributions and developments in the use of nanoparticles for photothermal therapy.[12−15] Photothermal therapy involves the use of near infrared (NIR) light having maximum tissue penetrability[16] that can be absorbed by nanoparticles to generate heat to kill cancer cells present in its vicinity. A number of nanoparticles in the form of gold-silica nanoshells,[12] gold nanorods,[14] gold−gold sulfide nanoparticles,[13] gold−iron oxide nanoparticles,[17] etc., have been developed and reported to exhibit photothermal activity. Such nanoparticles are specifically engineered through careful reaction processes such that they exhibit intense NIR absorptivity and stability. The reactants often used in such reaction processes are toxic and their remnants if present in the nanomedicine can cause systemic toxicity.[18,19] For example, in the synthesis of gold nanorods, cetyltrimethylammonium bromide (CTAB), whose cytotoxicity is well-known, is used as a capping agent to facilitate its directional synthesis process.[19,20] Therefore, in this regard, a completely aqueous and safe route of synthesis is a desirable attribute for nanoparticles to be used in vivo.

Green chemistry route has recently emerged in the past decade as a cheap and easy alternative method for the synthesis of metallic nanoparticles of gold and silver.[21] Different phytochemical reagents like lemongrass extract,[22] tea phytochemicals,[23] soybeans,[24] garlic extract,[25] grape seed extract,[26] etc., have been used for the synthesis of metallic or composite gold nanoparticles. Nanoparticles of different sizes and shapes synthesized by varying the reaction process parameters by these routes showed good stability, and biocompatibility.[25,27] For example, Shankar et al. have demonstrated that by varying the amount of lemon grass extract, anisotropic nanoparticles exhibiting NIR absorbance can be synthesized.[22] In this research, NIR absorbing

Received: January 15, 2014
Accepted: May 8, 2014
Published: May 8, 2014

   dx.doi.org/10.1021/am500302t | ACS Appl. Mater. Interfaces 2014, 6, 8080−8089

gold nanoparticles have been suggested for use in glass coatings as IR blockers for architectural applications. However, for utilizing such nanomaterials for biological applications as in photothermal therapy, their absorbance has to be maximum in the wavelength range where the tissue absorptivity is high, that is, 800−1000 nm.[16] Majority of the studies on green synthesized gold nanoparticles in literature focus mainly on their preparation and stabilization aspects, with limited thrust on its use in biology. Herein, using the extract of *Theobromo cacao* (cocoa), anisotropic gold nanoparticles have been synthesized and stabilized, without the use of any additional capping agents. Cocoa, according to the United States Department of Agriculture has one of the highest oxygen radical absorbance capacity (ORAC) value.[28] A high ORAC value is indicative of its strong reducing capability, thereby favoring its choice for gold nanoparticle synthesis from gold ion solution. The processing parameters that yielded nanoparticles with optimal optical absorbance were explored. A protocol for separating anisotropic nanoparticles from a mixture of spherical and anisotropic particles using density gradient centrifugation technique was optimized for achieving maximal NIR absorbance. The biocompatibility and efficacy of these anisotropic nanoparticles for photothermal therapy of cancer cells was evaluated. Further, the suitability of the nanoparticles for X-ray contrast applications was also analyzed.

MATERIALS AND METHODS

Materials. Gold chloride ($HAuCl_4$) was purchased from Spectrochem, India, sucrose from Qualigens, India, and unprocessed raw cocoa powder from Agro products and Agencies, Kottayam, Kerala. Mouse fibroblasts L929 cells, mouse embryonic fibroblast NIH-3T3 cells, human epidermoid carcinoma A431 cells and human breast cancer MDA-MB 231 cells were purchased from National Centre for Cell Sciences (NCCS), Pune, India. All other reagents and chemicals were used as obtained without any further purification and processing. All glasswares and magnetic stir bars were cleaned with Aqua Regia prior to use.

Methods. *Synthesis of Cocoa Extract Powder Solution.* Prior to nanoparticle preparation, cocoa extract solution was prepared. For this, 1 g of unprocessed cocoa powder was added to 200 mL of deionized water and stirred at 80 °C for 20 min to extract its hydrophilic components. The resultant solution was centrifuged for 15 min at 3000 rcf at 4 °C. The supernatant from this was collected and dried at 80 °C for obtaining the cocoa extract powder. This powder was then dissolved in deionized water to obtain the final reducing agent at a concentration of 10 mg/mL. The cocoa extract powder solution was autoclaved and stored in refrigerated conditions for further use.

Synthesis of Gold Nanoparticles. $HAuCl_4$ solution was prepared in Milli Q water and placed in a water bath under continuous stirring. Different volumes (200, 250, 270, and 300 μL) of cocoa extract powder solution were added to $HAuCl_4$ solution and the reaction was allowed to continue in controlled temperature conditions (30, 40, 50, 60, and 70 °C) for 15 min. After the reaction mixture attained room temperature, stirring was continued overnight to enable the completion of reaction yielding a purple colored crude nanoparticle suspension.

Anisotropic Gold Nanoparticle Separation. To separate anisotropic nanoparticles from the crude nanoparticle suspension, a sucrose based density gradient centrifugation was employed. Sucrose gradients were prepared in 50 mL falcon tubes by carefully layering 5 mL of sucrose solutions of decreasing concentrations one above the other (starting from 90%, 80%, 70%, ..., to 10%). The crude nanoparticle solution (5 mL) was then added above the sucrose gradient column and centrifugation was performed at 5000 rcf for 80 min at 4 °C temperature. After centrifugation, individual sucrose layers were separated carefully and washed repeatedly by centrifuging at 17000 rcf for 10 min. The particles were eventually resuspended in Milli Q water and probe sonicated for further experiments.

Nanoparticle Characterization. Surface plasmon resonance (SPR) of the prepared crude nanoparticle suspension as well as the separated anisotropic nanoparticles was recorded using a UV−vis−NIR spectrophotometer (Lambda 750, PerkinElmer, USA) to check the absorbance of Au nanoparticles in the wavelength range extending from 350 to 1200 nm. The size and morphology of the separated anisotropic gold nanoparticles that showed maximal NIR absorbance were evaluated using Transmission electron microscopy (TEM, CM200, Philips, Netherlands) at 200 kV accelerating voltage and field-emission scanning electron microscopy (FE-SEM, JEOL JSM-7600F, Japan) at 5 kV accelerating voltage. The samples for TEM were prepared by dropping a dilute solution of the nanoparticle on a 400 mesh copper grid, while that for FESEM were drop casted directly onto an aluminum foil placed on a stub. High-resolution TEM (HRTEM, JEOL 3010 UHR, Japan) was carried out to view the crystalline planes and to calculate the *d*-spacing of the nanoparticle. Crystallinity of the synthesized nanoparticles was evaluated using an X-ray diffraction equipment (XRD, X'Pert PRO, PANanalytical, Netherlands) fitted with a Cu$K\alpha$ source (λ = 1.54056 Å). Gold nanoparticle solution was drop casted onto a glass substrate yielding a thick film for spectral analysis in the range 5−80° at a step size of 0.02°. Phase identification was carried out with the help of standard JCPDS database. The surface charge and stability of the nanoparticles were assessed by analyzing its zeta potential using a Zeta potential equipment (DLS-ZP/Particle Sizer TM380 ZLS, Nicomp, USA). Fourier Transform Infrared Spectroscopy (FTIR) was used to determine the surface functional groups in the nanoparticle in the wavenumber range extending from 4400 to 400 cm^{-1} (Spectrum RX1 FT-IR Spectrometer, PerkinElmer, USA). Samples were prepared by mixing and pelletizing 2 mg of Au Nanoparticles with 175 mg of KBr. To further confirm the presence of functional groups on the nanoparticles, X-ray Photoelectron Spectroscopy (XPS, AXIS Ultra DLD, Kratos Analytical, United Kingdom) measurements were carried out which utilized an Al Kα source (photon energy, 1468.6 eV). The samples for XPS measurements were prepared by drop casting and air drying a small volume of nanoparticle suspension onto a glass coverslip.

Cell Culture Experiments. All cell culture reagents and plastic wares were purchased from Invitrogen Life Technologies (CA, USA). A431 and NIH-3T3 cells were maintained in Dulbecco's modified Eagles Medium (DMEM, Sigma-Aldrich, USA), while MDA-MB 231 and L929 cells were maintained in Minimum Essential Medium (MEM, Sigma-Aldrich, USA). Briefly, the cells were maintained in T-25 flasks in their respective medium with 10% fetal bovine serum (FBS, Invitrogen, CA, USA) containing 50 IU ml^{-1} penicillin and 50 μg mL^{-1} streptomycin. The cells were incubated in a biological incubator at 5% CO_2 in a humidified environment at 37 °C temperature. Upon reaching 80% confluency, the cells were split using 0.05% Trypsin-EDTA (Invitrogen, CA, USA) and reseeded into a T-25 flask with 5×10^5 cells seeding density. All cells were used for experimental procedures at least two splits after revival.

Cytotoxicity Studies and Particle Uptake. A431, MDA-MB 231,L929 and NIH-3T3 cells were trypsinized and seeded in 96-well plates at 5000 cells/well seeding density. Twenty-four hours post seeding, the cells were treated with different concentrations of anisotropic gold nanoparticles (5−200 μg/mL) prepared in cell culture media. Each concentration was analyzed in triplicates. Cells treated with triton X-100 served as positive controls, while untreated cells served as negative controls. After 24 h of treatment, the cells were washed with Phosphate buffer solution (PBS, pH = 7.4) and 10% Alamar blue solution made in basal medium was added in each well. The absorbance values were read in a microplate reader (BioRad Power Wave XS) after 4 h of incubation at 570 nm, with 600 nm set as reference. The % cell viability was calculated using the equation as follows

$$\%\text{cell viability} = \frac{\text{OD test}}{\text{OD control}} \times 100$$

Here, OD test denotes absorbance of test wells, while OD control denotes absorbance of negative control wells.

To quantify the uptake of anisotropic gold nanoparticles on cells, inductively coupled plasma atomic emission spectrometry (ICP-AES, Thermo Electron IRIS INTREPID II XSP DUO, USA) was utilized.

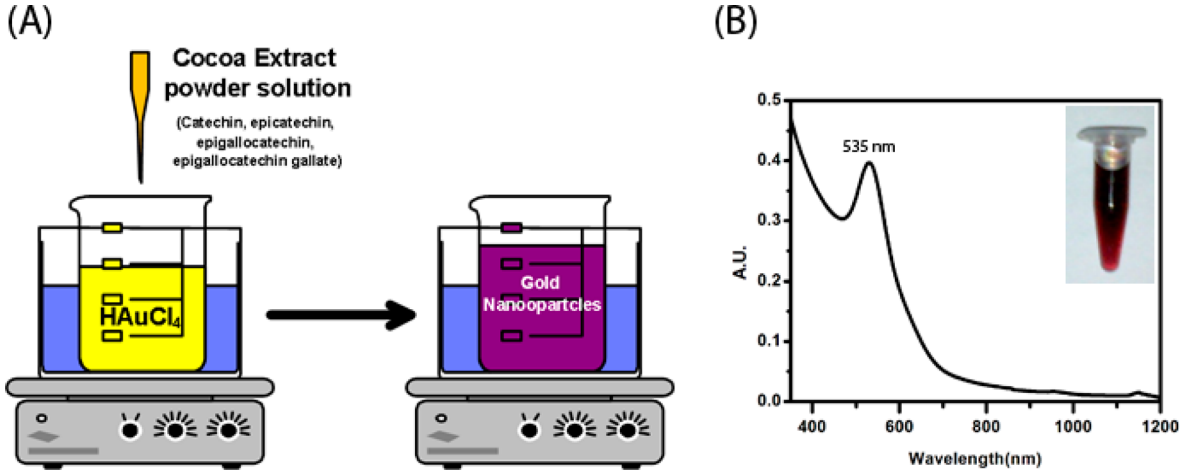

Figure 1. (A) Schematic of synthesis of gold nanoparticles using cocoa extract powder solution as reducing agent and $HAuCl_4$ solution as precursor. A controlled water bath is used to maintain uniform temperature conditions. (B) UV−vis−NIR absorption spectra of spherical gold nanoparticles showing characteristic absorption peak at 535 nm. Inset shows the purple red color of gold nanoparticles prepared using cocoa extract.

A431 cells were first cultured in 6-well plates at a seeding density of 0.3×10^6 cells/well for 24 h. These cells were then treated with 100 and 200 μg/mL nanoparticle concentrations in triplicates for 24 h. After treatment, the cells in each well were washed twice with PBS, followed by trypsinization and cell harvesting. The cell pellets were digested with 10% aqua regia and analyzed using ICP-AES. Untreated cells and nanoparticles alone served as controls.

Reactive Oxygen Species (ROS) Assay. 2′,7′-Dichlorodihydrofluorescein diacetate (H2DCFDA) is a cell permeable molecule that gets cleaved in the presence of intracellular ROS to generate a highly fluorescent 2′,7′-dichlorofluorescein molecule. The ROS levels induced in cells upon nanoparticle treatment were evaluated using flow cytometry (BD FACS Aria, USA). Briefly, A431 and NIH-3T3 cells were seeded into 6-well plates at 10^5 cells/well. Following cell attachment, the cells were treated with 100 μg/mL of anisotropic gold nanoparticles resuspended in cell culture media. After 24 h of treatment the cells were then trypsinized and resuspended in PBS at a final concentration of 5 μM H2DCFDA and incubated in dark for 30 min. The cells were then washed with PBS and analyzed using FACS.

In Vitro Photothermal Therapy. To determine the effectiveness of cell ablation by laser light due to NIR absorbing anisotropic gold nanoparticles, a laser scanning confocal microscopy system (Leica Confocal Microscope, DMI 6000 CS with Leica TCS SPSII scanner) equipped with a mode locked Ti:sapphire multiphoton laser (Spectra Physics, Mai Tai Scientific, USA) was employed. The wavelength of the output beam was tunable to match the absorption of the anisotropic nanoparticles. The femtosecond pulses from the Ti:sapphire laser operating at 800 nm at a power of 36 mW was used for the photothermal ablation of cancer cells using a 20× objective for 10 min [NA = 0.7, scan rate of 400 kHz and 1024 × 1024 resolution, with a total scan area of 775 × 775 μm^2].

A431 cancer cells were cultured on 96 well plates (BD, black well, clear bottom, imaging plate) at 5,000 cells/well for 24 h. Varying concentrations of anisotropic gold nanoparticles (50 to 200 μg/mL) were then added to the wells and incubated for 24 h. After incubation, the cells were washed with PBS and fresh media was added before laser treatment. Untreated cells served as negative controls.

To validate cell death because of laser exposure, a live/dead staining was done using acrydin orange (AO)/ethidium bromide (ETBR) dye mixture. AO/ETBR staining is used for discriminating between live and dead cells based on cellular membrane integrity. AO is a cell permeant nuclear-acid binding dye that fluoresces green while ETBR is a cell impermeant nuclear acid binding dye which fluoresces red. Dead cells which lose their membrane integrity can fluoresce red because of the intercalation of ETBR with its DNA. AO/ETBR dye at a ratio of 3 μg/mL AO and 10 μg/mL ETBR in PBS was prepared as the working standard solution. One μL of this dye mixture was added directly into culture wells containing 100 μL media. The cells were then incubated with the dye for 30 min and then viewed directly under confocal microscope using an excitation source of 488 nm Ar laser.

CT Contrast Imaging. To investigate the suitability of anisotropic gold nanoparticles for CT imaging, a clinically used SOMATOM Sensation Cardiac 64 CT scanner (Siemens) was used. The anisotropic nanoparticles were placed into 96 well plates at concentrations starting from 0.1 to 2 mg/mL. Omnipaque, a clinically approved CT contrast agent was used as a reference, while Milli Q water served as the negative control. The instrument was operated at a tube voltage of 100 kV_p, tube current of 200 μA, scan time of 6.97 s, slice thickness of 5 mm, and rotation time of 1 s. Manually selected regions of interest of equal diameter were used to determine the Hounsfield units of each well for comparison of X-ray contrast measurements.

RESULT AND DISCUSSION

Nanoparticle Synthesis and Characterization. *Theobromo cacao*, commonly called as cocoa, contains various polyphenols,[33] such as catechin, epicatechin, epigallocatechin, epigallocatechin gallate, and procyanidin, which are strong reducing agents. In the present work, gold nanoparticles were synthesized using cocoa as a reducing agent at varying experimental conditions as shown in Figure 1 A. One of the characteristic signatures of gold nanoparticles is its absorption spectrum in the VIS-NIR region because of the phenomenon of SPR,[29] which varies with nanoparticle size and shape.[30,31] Upon addition of the reducing agent, the color of the precursor solution changed gradually from yellow to black and then to purple red. Figure 1 B shows the UV−vis−NIR spectrum of the synthesized gold nanoparticles obtained by the addition of 500 μL of the cocoa extract powder solution to 1 mM $HAuCl_4$ solution at 37 °C room temperature. The color change of the precursor solution from yellow to black represents the initial nucleation stage, wherein small sized unstable gold seeds are produced due to the reduction of gold ions initiated by the cocoa extract powder solution. As the seeds grow in size to form stable nanosized particles, the color of the solution changes from black to purple red, which in turn results in the characteristic SPR absorbance at 535 nm representative of gold nanoparticles. The gold nanoparticles were found to be stable even after repeated centrifugation and washing. Thus, cocoa extract possessed the dual role of reducing gold ions and providing stabilization effects to the formed nanoparticles. This stability is conferred by the

dx.doi.org/10.1021/am500302t | ACS Appl. Mater. Interfaces 2014, 6, 8080−8089

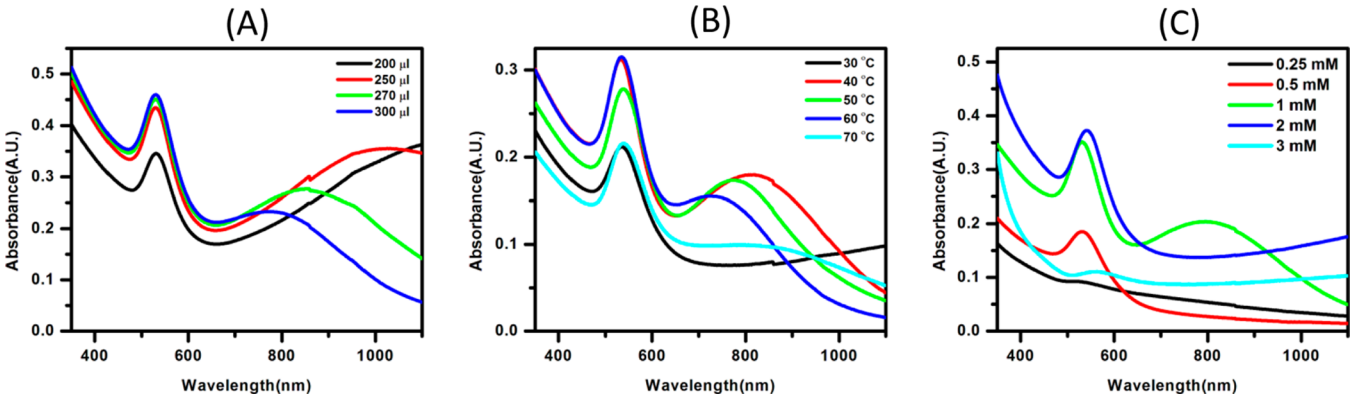

Figure 2. UV−vis−NIR spectrum of synthesized gold nanoparticles with (A) variation in reducing agent volume at constant temperature of 37 °C and 1 mM $HAuCl_4$ precursor solution (B) variation in reaction temperature at constant reducing agent volume of 270 μL and 1 mM $HAuCl_4$ precursor concentration (C) variation in precursor concentration at constant reducing agent volume of 270 μL and 40 °C temperature.

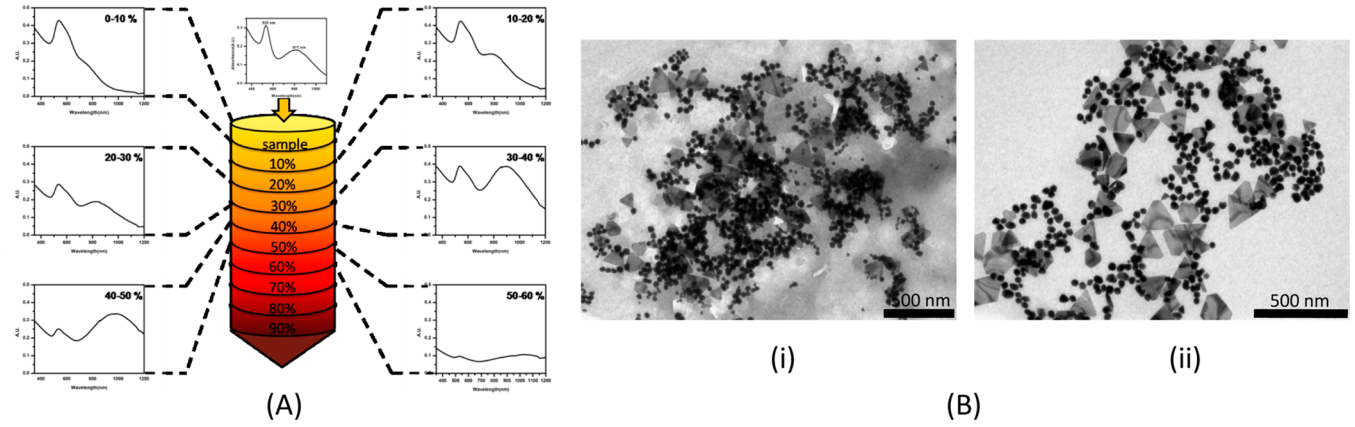

Figure 3. (A) Schematic representing spectral absorbance of separated nanoparticle fraction in each sucrose layer. Appreciable NIR absorbance can be observed in the nanoparticles accumulated in the 40−50% sucrose layer (B) TEM images of (i) gold nanoparticle mixture and (ii) gold nanoparticles obtained from 40% to 50% sucrose layer.

polyphenolic groups of the reducing agent, namely, cocoa, which would be substantiated by the FTIR data in the ensuing section.

Further, the reaction parameters, namely, amount of cocoa extract, temperature and precursor concentration, were varied as shown in Figure 2 to analyze its effects on the morphology and size of gold nanoparticles. Generally, for spherical nanoparticles, an increase in size leads to a red-shift of its SPR in the visible region of the electromagnetic spectrum. On the other hand, a change in shape of the gold nanoparticles away from its low free energy state of isotropy (spherical structure) leads to the development of a longitudinal surface plasmon resonance (LSPR) peak in the far-visible or NIR region.[31] Thus, for the analysis of the prepared nanoparticles, absorption spectroscopy was used for process optimization to synthesize NIR absorbing gold nanoparticles for photothermal therapy.

Figure 2 A shows the variation in spectral absorbance of the gold nanoparticles with varying amounts of reducing agent. With decreasing amount of reducing agent, the peak NIR absorbance due to LSPR red-shifted with increasing intensity. Similar results have also been reported earlier for the preparation of gold nanoparticles using lemon grass[27] and garlic extracts.[25] This behavior was attributed to the lower rate of synthesis of nanoparticle seed than the rate of its sintering, yielding particles of anisotropic nature. In our experiment, cocoa extract may contain higher amounts of reducing agents as compared to stabilizing agents, which when used at low concentrations, yields several unstabilized smaller nanoparticles. These then coalesce together to form larger but stable anisotropic nanoparticles. On the other hand, higher concentrations of cocoa extract resulted in stable small sized spherical nanoparticles. An extract volume of 270 μL yielded nanoparticles with an optimal optical absorbance at 800 nm and hence was selected for further optimization.

Figure 2 B shows the variation in the absorbance spectrum of the synthesized nanoparticles with increasing reaction temperatures at the extract volume of 270 μL. At 30 °C, in addition to the typical SPR absorbance peak in the visible region at 535 nm a weak absorption in the NIR region was observed. Upon increasing the reaction temperature to 40 °C, a relatively prominent maxima in the NIR region was formed. Further increase in temperature led to blue shifting of the NIR absorbance with reduction in the absorbance intensity. With increasing temperature, the increased rate of reduction and stabilization would outweigh the rate of coalescence of smaller unstabilized nanoparticles, thereby producing larger number of smaller stabilized anisotropic nanoparticles as evinced by the blue shift of the NIR absorbance. Hence, for an extract volume of 270 μL, the processing temperature was optimized at 40 °C for maximal NIR absorbance.

Figure 2 C depicts the absorbance profile of the nanoparticles obtained after reduction using different precursor concentration of $HAuCl_4$. At 0.25 and 0.5 mM precursor concentrations, low intensity SPR absorbance peak at 535 nm was observed, which is

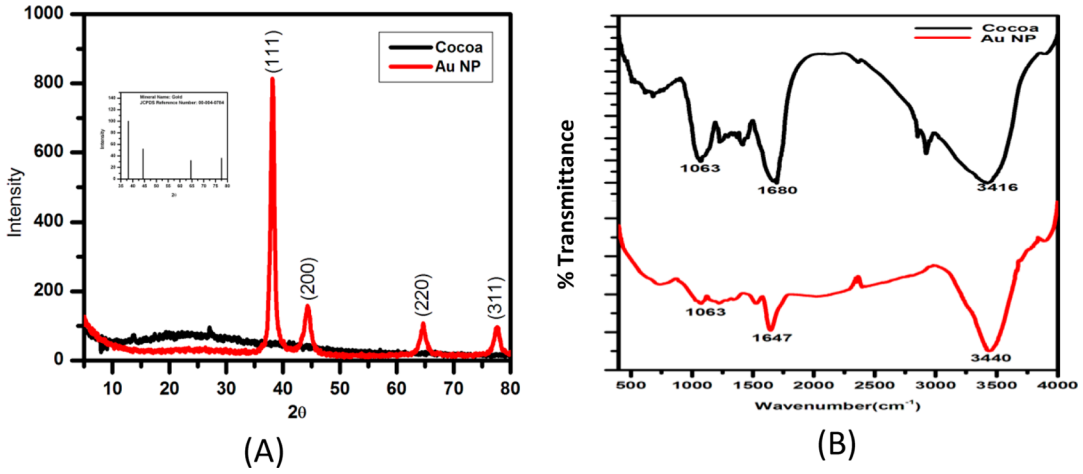

Figure 4. (A) XRD of anisotropic gold nanoparticles and cocoa powder. Anisotropic gold nanoparticles show characteristic diffraction peaks of crystalline gold, while cocoa powder shows no diffraction peaks. Inset shows XRD spectrum of metallic gold from the JCPDS database. (B) FTIR of cocoa and anisotropic gold nanoparticles.

indicative of the formation of low concentrations of spherical gold nanoparticles. As precursor concentration was increased to 1 mM, a fraction of anisotropic nanoparticles formed, with characteristic absorbance in the NIR region (700−1000 nm). Such anisotropic nanoparticles form when the excess left over precursor is reduced, but not well stabilized by the limited concentration of stabilizing agents. With further increase in precursor concentration to 3 mM, the number of precursor molecules per unit volume increased as compared to the reducing agent concentration, thereby inhibiting the complete reduction reaction. Hence, an optimal concentration of 1 mM $HauCl_4$ precursor, 40 °C reaction temperature, and 270 μL cocoa extract volume were selected for the synthesis of anisotropic nanoparticles for further experiments.

To improve the anisotropic nanoparticle concentration and thereby obtain particles with maximum NIR absorbance, sucrose density gradient centrifugation was employed. Figure 3 A shows the absorbance spectra of the nanoparticles in each sucrose layer after centrifugation. From the figure, it can be observed that the intensity of absorbance due to the longitudinal and transverse SPR in each sucrose layer was different. It is evident that as the concentration of sucrose increased, the absorbance intensity of LSPR increased and SPR decreased. This variation can be explained due to the differences in the migration rates of anisotropic nanoparticles as compared to spherical nanoparticles in sucrose, owing to their variations in size and shape. This absorbance profile is further supported by the TEM images shown in Figure 3B, wherein it was observed that the concentration of spherical nanoparticles after sucrose density gradient centrifugation has reduced considerably, thus giving higher LSPR peak intensity values. From the TEM measurements it can be seen that the anisotropic gold nanoparticle fraction has a size range of 150−200 nm which corroborated with the hydrodynamic diameter values (150 ± 20 nm) obtained from dynamic light scattering. To further confirm the improvement in the anisotropic nanoparticle fraction, FE-SEM of nanoparticles obtained in the 0−10% and 40−50% sucrose layers was also carried out (Figure S1, Supporting Information). The figure clearly demonstrates the improvement of the concentration of anisotropic nanoparticles over spherical nanoparticles upon density gradient centrifugation.

X-ray diffraction of the anisotropic gold nanoparticles showed all the characteristic peaks of metallic gold as shown in Figure 4 A. The presence of distinct peaks in the XRD pattern signifies that the cocoa-reduced gold nanoparticles were highly crystalline in nature. Further, peak broadening implies the small nanocrystallite size of the synthesized nanoparticles. In comparison, cocoa exhibited a clearly amorphous XRD pattern. The high crystallinity of the prepared particles was additionally analyzed by HRTEM for different anisotropic gold morphologies. Figure S2 (Supporting Information) depicts the HRTEM images which display the highly ordered crystalline planes with a *d*-spacing value of 2.27 Å (for prismatic and quasi-spherical nanoparticles) and 2.32 Å for rod-like structures. This correlated well with the lattice spacing of spherical nanoparticles shown in Supporting Information Figure S2 (D), as well as other literature reports,[38] implying that green route enabled the synthesis of crystalline gold nanoparticles.

The particles were further analyzed using FTIR as shown in Figure 4B to determine the functional groups present in green synthesized gold nanoparticles. On comparing the FTIR spectra of cocoa powder and gold nanoparticles, it is evident that there exist three distinctive overlapping peaks. The broad peak ranging from 4000 to 3000 cm^{-1} corresponded mainly to the hydroxyl (−OH) functional group stretching, that at 2900 cm^{-1} to the long chain hydrocarbon groups, 1700 to 1600 cm^{-1} represented the carbonyl functional group stretching, and the 1063 cm^{-1} in the fingerprint region corresponded to the aromatic ring groups. These functional groups are typical of cocoa and have been published elsewhere.[32] The FTIR spectrum of cocoa reduced gold nanoparticles revealed spectral bands that overlapped with cocoa. The presence of the 1063 cm^{-1} band and the absence of the 2900 cm^{-1} band in gold nanoparticles clearly signified that the polyphenols and not the long chain hydrocarbon groups were the major constituents that acted as stabilizer molecules. The corresponding carbonyl group signatures of the polyphenols were also present in the gold nanoparticle as a band in the 1700 to 1600 cm^{-1} window confirming our hypothesis. Such a polyphenolic coating on nanoparticles produced a high zeta potential value of −50 ± 8 mV, which is also a measure of its high colloidal stability in aqueous systems.

To further confirm the presence of polyphenol coating on the nanoparticle, XPS analysis was performed. Figure 5 A shows the

dx.doi.org/10.1021/am500302t | ACS Appl. Mater. Interfaces 2014, 6, 8080−8089

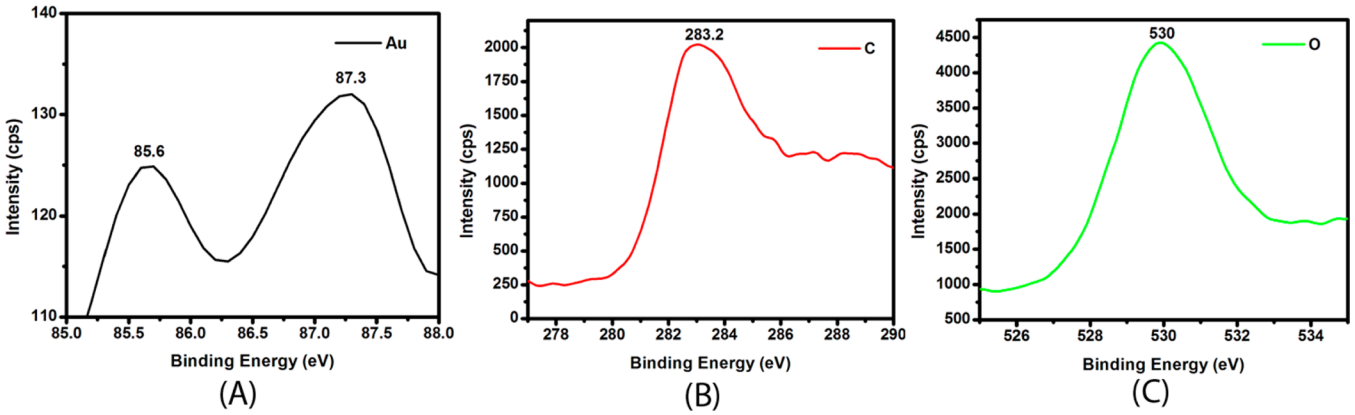

Figure 5. XPS of anisotropic gold nanoparticles depicting (A) Au $4f_{7/2}$ and Au $4f_{5/2}$core levels at 85.6 and 87.3 eV, repectively, (B) C 1s at 283.2 eV, and (C) O 1s at 530 eV.

resolved spectra of the core levels of Au, namely, $4f_{7/2}$ and $4f_{5/2}$ at 85.6 and 87.3 eV, respectively, correlating well with the literature values of metallic Au(0).[27,39] Figure 5B and C represent the spectra obtained for C 1s and O 1s, respectively. The C 1s peak at 283.2 eV and O 1s peak at 530 eV can be due to the presence of aromatic hydrocarbon groups as well as the carbonyl groups present in polyphenols which stabilized the gold nanoparticles.[27,40] The presence of such high intensity peaks of C and O in XPS further corroborates the results obtained from FTIR analysis.

BIOLOGICAL STUDIES

The cytocompatibility of the green synthesized anisotropic nanoparticles were tested on A431, MDA-MB 231, L929, and NIH-3T3 cell lines. Figure 6 represents the % cell viability plotted against nanoparticle concentration for a treatment period of 24 h.

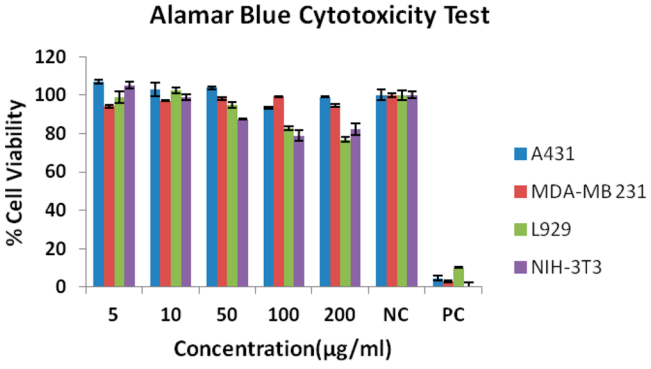

Figure 6. % Cell viability assessment as a function of nanoparticle concentration for a treatment period of 24 h. NC represents untreated controls, while PC represents cells treated with 0.1% Triton X-100.

From Figure 6 it can be seen that the nanoparticles showed good cytocompatibility for a treatment period of up to 24 h for a maximum concentration of 200 μg/mL, with a slight reduction (~80%) in % cell viability observed for L929 and NIH-3T3 cells at the highest tested dose. The cytocompatibility can be attributed to the dense polyphenolic coating on the nanoparticles synthesized by the green route. The polyphenolic stabilization that provided biocompatibility, coupled with its NIR absorbance, make these anisotropic gold nanoparticles a good choice for photothermal therapy, unlike the gold nanorods stabilized by cytotoxic CTAB.

To further evaluate its cytocompatibility, ROS assay was performed which measures the production of intracellular ROS. A431 and NIH-3T3 cells were treated with 100 μg/mL of anisotropic gold nanoparticles for 24 h and then incubated with cell permeant dye DCFH-DA for 30 min. Figure 7 shows the % cells that showed intracellular ROS activity as compared to control cells that are not treated with nanoparticles.

Percentage of A431 cells that showed an ROS response were 5.6% and 2.4% for control and test samples, while that for NIH 3T3 were 4.4% and 4.2%, respectively. Thus, the ROS generated by the gold nanoparticles in both cell types was very low indicating that the nanoparticles were cytocompatible and did not contribute toward any stress induced intracellular ROS generation. Polyphenols are considered as good ROS scavengers,[33] and the presence of a polyphenolic coating on the nanoparticles could have mitigated the generation of ROS, which could otherwise have hampered cellular functioning and induced DNA damage.

Cellular uptake of Au nanoparticles was confirmed by ICP-AES analysis on A431 cells at two different particle concentrations. An initial ICP analysis of bare nanoparticles revealed that 100 μg of Au nanoparticles contained ~55 ug of gold ions after acid digestion. Figure 8 depicts the variation in cellular uptake of nanoparticles at 24 h expressed as % particle uptake. The results revealed that nearly 47% and 67% of particles accumulated within the cells for 100 and 200 μg/mL nanoparticle concentrations, respectively. Thus, the high uptake of NIR absorbing anisotropic nanoparticles by A431 cells can help in inducing photothermal damage upon laser exposure.

In Vitro Photothermal Therapy. Figure 9A and B represent the DIC images of A431 cells treated with 100 μg/mL of anisotropic gold nanoparticles for 24 h before and after laser irradiation respectively, while Figure 9D and E depict the same for untreated A431 cells before and after irradiation. From the figures, it is clearly evident that the nanoparticle treated cells underwent an extensive morphological change after laser irradiation in the form of cellular appendage withdrawal and cell membrane rupture, leading to cell blebbing and the discharge of cytoplasmic fluid (depicted by arrows in Figure 9B and C). The maximal photothermal damage was observed in cells at the periphery of the cell colony. On the other hand, untreated cells showed no visible morphological changes after laser irradiation. Thus, cells treated with anisotropic gold nanoparticles for 24 h

dx.doi.org/10.1021/am500302t | ACS Appl. Mater. Interfaces 2014, 6, 8080−8089

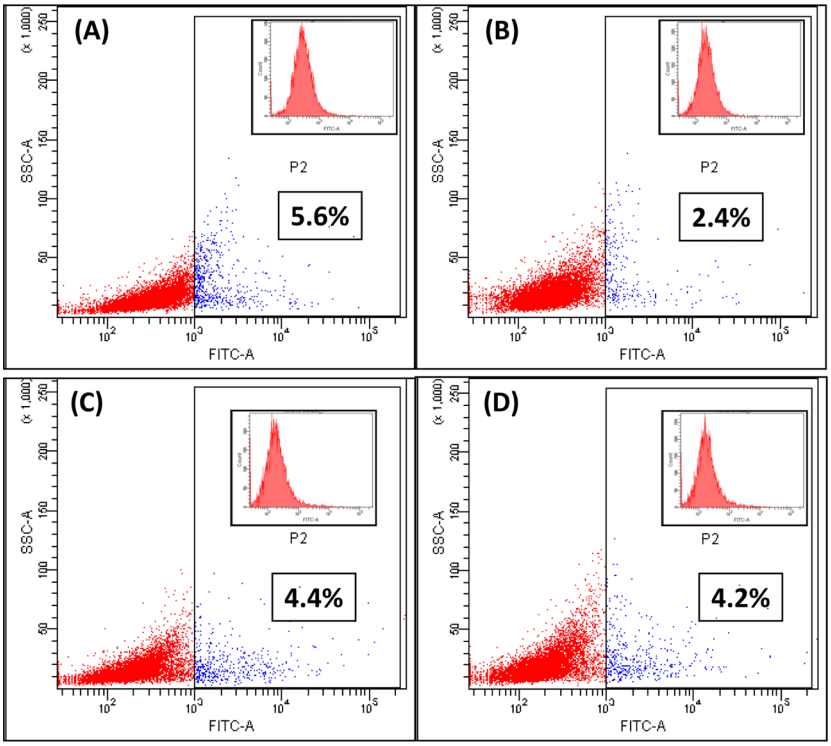

Figure 7. Scatter plot of Intracellular ROS activity of cells treated with nanoparticles using FACS. ROS activity is represented as the percentage of cells showing fluorescence resulting from DCF per 10,000 events. Panels A and B represent A431 cells as control and nanoparticle treated (100 μg/mL) respectively. Panels C and D represent NIH-3T3 cells as control and nanoparticle treated (100 μg/mL) respectively.

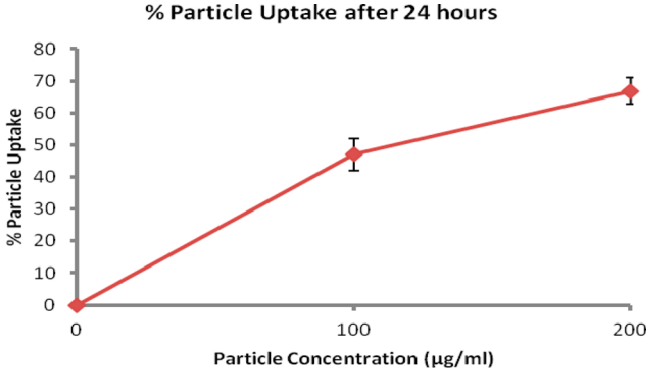

Figure 8. Graph demonstrating gold nanoparticle uptake by A431 cells after 24 h incubation with 100 and 200 μg/mL particle concentrations obtained from ICP-AES. Percentage of particles taken up was calculated using nanoparticle controls.

showed responsiveness to NIR laser irradiation. This can be attributed to the accumulation of NIR absorbing nanoparticles in the cells which would lead to the generation of highly localized photothermal effects within the cellular microenvironment upon laser irradiation, thereby leading to cell death. Thus, our studies demonstrated that a polydisperse mixture of anisotropic gold nanoparticles sufficed in developing photoinduced thermal damage on cancer cells.

Figure 10A–C represents the fluorescence confocal images after live/dead staining of A431 cells pretreated for 24 h with 200, 100, and 50 μg/mL of anisotropic nanoparticles after laser irradiation (36 mW for 10 min). It can be seen that the cells treated with 200 μg/mL of anisotropic gold nanoparticles and then exposed to NIR laser, showed maximum cell death at the laser spot of 775 × 775 μm^2 as shown in Figure 10 A, which was comparatively less at lower particle concentration. On the contrary, cells not treated with nanoparticles, but exposed to laser irradiation (Figure 10 D) showed no signs of cytotoxicity, implying the role of nanoparticles in photothermal therapy. Similarly, cells treated with nanoparticles alone at 100 μg/mL (Figure 10 E) without any laser irradiation did not impart any cell death, which was clearly evident from the green fluorescence of the viable cells. This also corroborated with the cytotoxicity assay performed on nanoparticle treated A431 cells, which showed high % cell viability.

The laser power density of 6 W/cm^2 used in the present study is much lesser than the fluence reported in studies using gold-based nanoparticles such as gold nanorods[14] (10 W/cm^2), gold-silica nanoshells[34] (80 W/cm^2), gold–gold sulfide nanoparticles[13] (25 W/cm^2), but comparable to gold hybrid nanoparticles[35] (5.1 W/cm^2). These results demonstrate the feasibility of using anisotropic nanoparticles with NIR absorbance synthesized by a simple green route for photothermal applications at low fluences.

CT Contrast of Anisotropic Gold Nanoparticles. The feasibility of using the green synthesized anisotropic gold nanoparticles as a X-ray contrast agent was analyzed in comparison to the clinically approved Omnipaque (polyiodinated aromatic compound) as control. Experiments were carried out at equal concentrations of the two materials as well as measurement conditions at 100 kV_p tube voltage.

Figure 11A depicts the CT contrast images of anisotropic gold nanoparticles in comparison to Omnipaque. It can be seen that at concentrations higher than 0.5 mg/mL, anisotropic gold nanoparticles showed a visibly brighter contrast as compared to Omnipaque, which was also quantitatively measured in Hounsfield units (Figure 11B). It can be seen that anisotropic gold nanoparticles showed signal intensity nearly 1.5 times

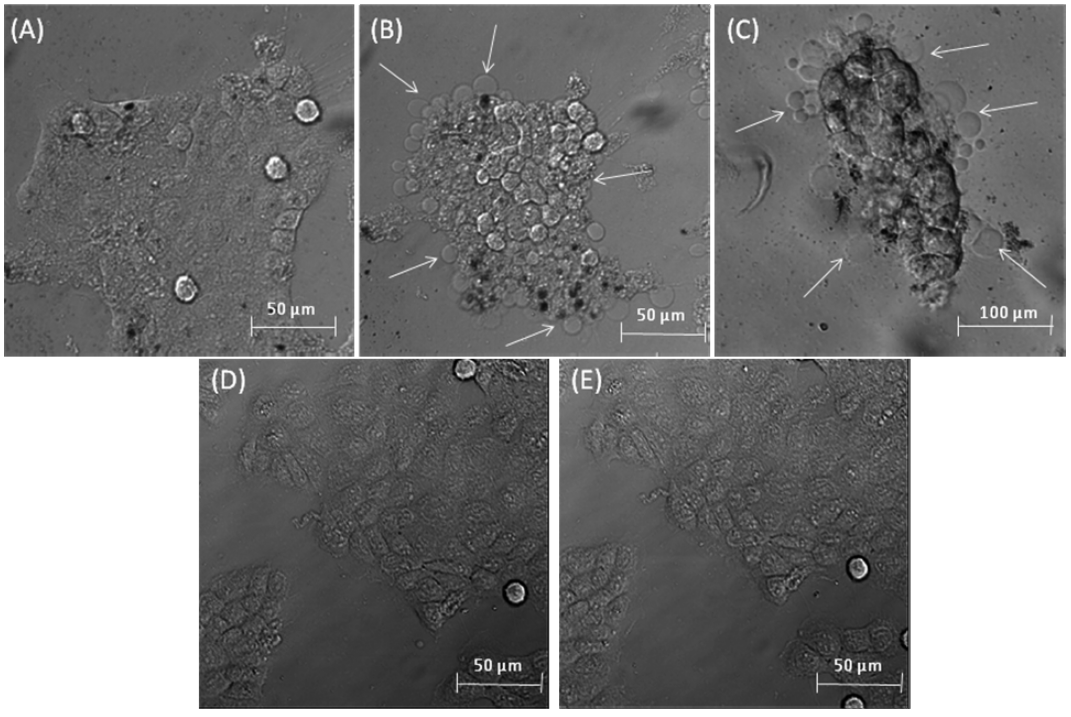

Figure 9. DIC images of A431 cells before (A and D) and after (B, C, and E) laser irradiation. Top panel represents cells treated with anisotropic gold nanoparticles at 100 μg/mL for 24 h and bottom panel the untreated controls. Changes in cell morphology including cell membrane withdrawal and membrane disruption were observed (represented in arrows in B and C) after laser irradiation at 36 mW for 10 min. (C) represents high magnification image of nanoparticle treated cells after laser irradiation. No morphological changes were noticed in control samples after laser irradiation.

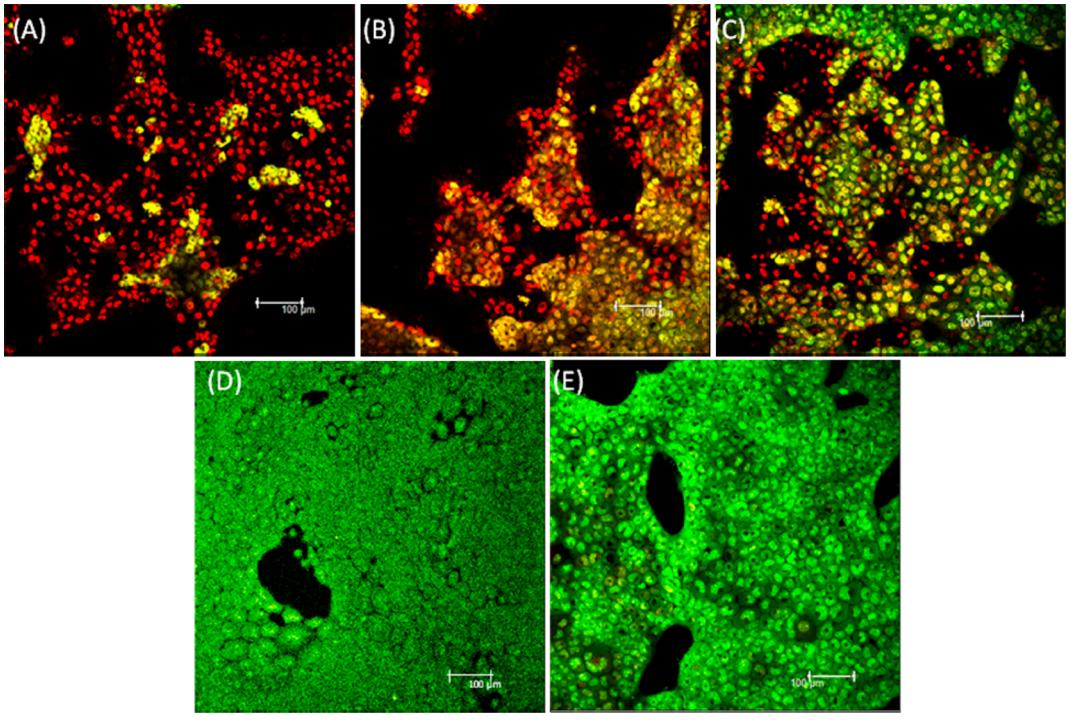

Figure 10. Live/dead staining of A431 cells after 800 nm laser irradiation for 10 min at power = 36 mW. Nanoparticle concentration in panels A, B, C, and D are 200, 100, 50, and 0 μg/mL respectively. Decreasing amounts of red fluorescence is obtained with lower concentration of nanoparticles which indicates the photothermal activity of the nanoparticles in cell killing. (E) Live/dead staining of A431 cells treated with 100 μg/mL nanoparticle concentration without laser treatment.

greater than that of Omnipaque at same material concentrations. Owing its higher atomic number, gold attenuates X-rays more effectively than iodine and therefore produces superior contrast.[36] This enhanced CT contrast offered by gold nanoparticle can be of clinical significance since lower concentration of nanoparticle maybe used to obtain the desired effects within the body. Thus, the use of green synthesized biocompatible anisotropic nanoparticles can help in alleviating

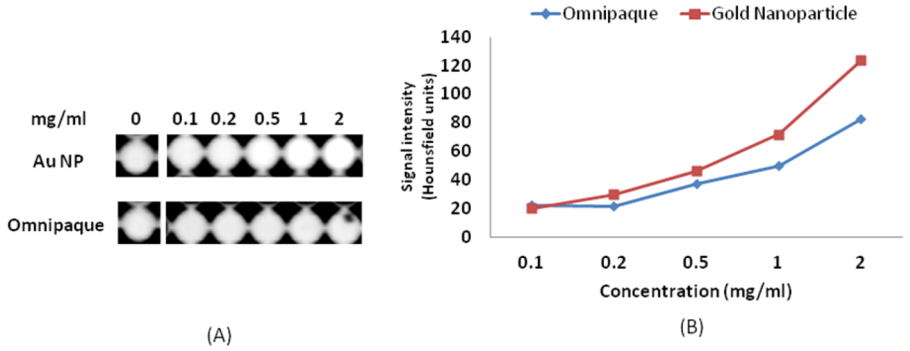

Figure 11. (A) Comparison of CT contrast images of anisotropic gold nanoparticle and Omnipaque with increasing concentrations. Brighter images are obtained for higher concentration of anisotropic gold nanoparticles. (B) Graph depicting variations of computed HU value of anisotropic gold nanoparticle and Omnipaque with increasing concentrations.

the cytotoxicity associated with the use of clinically used polyiodinated aromatic compounds like Omnipaque.[37]

CONCLUSIONS

Conventionally, NIR absorbing gold nanoparticles for use in photothermal therapy are synthesized using complex schemes that employ nonbiocompatible reagents, which causes toxicity concerns in vivo. We have optimized a facile green route for preparing anisotropic gold nanoparticles using cocoa as the reducing and stabilizing agent, which displayed characteristic NIR absorption. Owing to the polyphenolic coating imparted by cocoa, these anisotropic gold nanoparticles showed high colloidal stability and cytocompatibility in vitro. The anisotropic particles exhibited good photothermal activity upon femtosecond laser exposure at 800 nm on A431 cancer cells at low fluence. The cells displayed a characteristic blebbing indicative of apoptosis upon laser irradiation, which was absent for the irradiated cells, which are devoid of nanoparticle treatment. This was further confirmed by the live−dead imaging of nanoparticle treated cells after laser exposure which showed greater amounts of cell death at higher gold concentrations. The usefulness of the green synthesized anisotropic gold nanoparticles for CT imaging was assessed to be high in comparison to Omnipaque. Thus, our study demonstrated that green synthesized, polydispersed anisotropic gold nanoparticles can be used effectively as a dual photothermal therapeutic agent and a CT diagnostic agent for biomedical applications.

ASSOCIATED CONTENT

Supporting Information

Additional FE-SEM and HR-TEM data. This material is available free of charge via the Internet at http://pubs.acs.org.

AUTHOR INFORMATION

Corresponding Author

*Fax: +91 484 2802030. Tel: +91 484 4008750. E-mail: deepthymenon@aims.amrita.edu.

Notes

The authors declare no competing financial interest.

ACKNOWLEDGMENTS

The authors would like to acknowledge Department of Science & Technology GOI, Nanomission initiative and the Nanotheragnostics Grant (SR/NM/NS-99/2009), for financial support and AIMS, Kochi for infrastructural support. The Sophisticated Analytical Instrumentation Facility at IIT Bombay is acknowledged for TEM and FE-SEM measurements. The Sophisticated Test and Instrumentation Centre at CUSAT is acknowledged for ICP-AES measurements. The Department of Physics at IIT Madras is acknowledged for HRTEM analysis. Authors also thank Mr. Sajin P. Ravi for his support in FTIR measurements, Mr. Sarath for confocal microscopy, and Mrs. Sreerekha P. R. for FACS analysis.

REFERENCES

(1) Zhang, Y.; Chan, H. F.; Leong, K. W. Advanced Materials and Processing for Drug Delivery: The Past and the Future. *Adv. Drug Delivery. Rev.* **2013**, *65*, 104−20.

(2) Laurent, S.; Dutz, S.; Häfeli, U. O.; Mahmoudi, M. Magnetic Fluid Hyperthermia: Focus on Superparamagnetic Iron Oxide Nanoparticles. *Adv. Colloid Interface Sci.* **2011**, *166*, 8−23.

(3) Kennedy, L. C.; Bickford, L. R.; Lewinski, N. a; Coughlin, A. J.; Hu, Y.; Day, E. S.; West, J. L.; Drezek, R. a A New Era for Cancer Treatment: Gold-Nanoparticle-Mediated Thermal Therapies. *Small* **2011**, *7*, 169−83.

(4) Kruse, D. E.; Stephens, D. N.; Lindfors, H. a; Ingham, E. S.; Paoli, E. E.; Ferrara, K. W. A Radio-Frequency Coupling Network for Heating of Citrate-Coated Gold Nanoparticles for Cancer Therapy: Design and Analysis. *IEEE Trans. Biomed. Eng.* **2011**, *58*, 2002−12.

(5) Xu, Y.; Mahmood, M.; Li, Z.; Dervishi, E.; Trigwell, S.; Zharov, V. P.; Ali, N.; Saini, V.; Biris, A. R.; Lupu, D.; Boldor, D.; Biris, A. S. Cobalt Nanoparticles Coated with Graphitic Shells as Localized Radio Frequency Absorbers for Cancer Therapy. *Nanotechnology* **2008**, *19*, 435102.

(6) Gannon, C. J.; Patra, C. R.; Bhattacharya, R.; Mukherjee, P.; Curley, S. A Intracellular Gold Nanoparticles Enhance Non-Invasive Radiofrequency Thermal Destruction of Human Gastrointestinal Cancer Cells. *J. Nanobiotechnol.* **2008**, *6*, 2.

(7) Moran, C. H.; Wainerdi, S. M.; Cherukuri, T. K.; Kittrell, C.; Wiley, B. J.; Nicholas, N. W.; Curley, S. A.; Kanzius, J. S.; Cherukuri, P. Size-Dependent Joule Heating of Gold Nanoparticles Using Capacitively Coupled Radiofrequency Fields. *Nano Res.* **2010**, *2*, 400−405.

(8) Walling, M. a; Novak, J. a; Shepard, J. R. E. Quantum Dots for Live Cell and in Vivo Imaging. *Int. J. Mol. Sci.* **2009**, *10*, 441−91.

(9) Thorek, D. L. J.; Chen, A. K.; Czupryna, J.; Tsourkas, A. Superparamagnetic Iron Oxide Nanoparticle Probes for Molecular Imaging. *Ann. Biomed. Eng.* **2006**, *34*, 23−38.

(10) Yim, H.; Seo, S.; Na, K. MRI Contrast Agent-Based Multifunctional Materials: Diagnosis and Therapy. *J. Nanomater.* **2011**, *2011*, 1−11.

(11) Qiao, R.; Yang, C.; Gao, M. Superparamagnetic Iron Oxide Nanoparticles: From Preparations to in Vivo MRI Applications. *J. Mater. Chem.* **2009**, *19*, 6274.

(12) Hirsch, L. R.; Stafford, R. J.; Bankson, J. a; Sershen, S. R.; Rivera, B.; Price, R. E.; Hazle, J. D.; Halas, N. J.; West, J. L. Nanoshell-Mediated

Near-Infrared Thermal Therapy of Tumors Under Magnetic Resonance Guidance. *Proc. Natl. Acad. Sci. U. S. A.* **2003**, *100*, 13549−54.
(13) Day, E. S.; Bickford, L. R.; Slater, J. H.; Riggall, N. S.; Drezek, R. a; West, J. L. Antibody-Conjugated Gold-Gold Sulfide Nanoparticles as Multifunctional Agents for Imaging and Therapy of Breast Cancer. *Int. J. Nanomed.* **2010**, *5*, 445−454.
(14) Huang, X.; El-Sayed, I. H.; Qian, W.; El-Sayed, M. A. Cancer Cell Imaging and Photothermal Therapy in the Near-Infrared Region by Using Gold Nanorods. *J. Am. Chem. Soc.* **2006**, *128*, 2115−20.
(15) Au, L.; Zheng, D.; Zhou, F.; Li, Z.-Y.; Li, X.; Xia, Y. A Quantitative Study on the Photothermal Effect of Immuno Gold Nanocages Targeted to Breast Cancer Cells. *ACS Nano* **2008**, *2*, 1645−52.
(16) Weissleder, R. A Clearer Vision for in Vivo Imaging. *Nat. Biotechnol.* **2001**, *19*, 316−7.
(17) Melancon, M. P.; Lu, W.; Zhong, M.; Zhou, M.; Liang, G.; Elliott, A. M.; Hazle, J. D.; Myers, J. N.; Li, C.; Stafford, R. J. Targeted Multifunctional Gold-Based Nanoshells for Magnetic Resonance-Guided Laser Ablation of Head and Neck Cancer. *Biomaterials* **2011**, *32*, 7600−8.
(18) Yang, Z.; Liu, Z. W.; Allaker, R. P.; Reip, P.; Oxford, J.; Ahmad, Z.; Ren, G. A Review of Nanoparticle Functionality and Toxicity on the Central Nervous System. *J. R. Soc., Interface* **2010**, *7* (Suppl 4), S411−22.
(19) Alkilany, A. M.; Murphy, C. J. Toxicity and Cellular Uptake of Gold Nanoparticles: What We Have Learned so Far? *J. Nanopart. Res.* **2010**, *12*, 2313−2333.
(20) Alkilany, A. M.; Nagaria, P. K.; Hexel, C. R.; Shaw, T. J.; Murphy, C. J.; Wyatt, M. D. Cellular Uptake and Cytotoxicity of Gold Nanorods: Molecular Origin of Cytotoxicity and Surface Effects. *Small* **2009**, *5*, 701−8.
(21) Kharissova, O. V.; Dias, H. V. R.; Kharisov, B. I.; Pérez, B. O.; Pérez, V. M. J. The Greener Synthesis of Nanoparticles Trends. *Biotechnology* **2013**, *31*, 240−8.
(22) Shankar, S. S.; Rai, A.; Ankamwar, B.; Singh, A.; Ahmad, A.; Sastry, M. Biological Synthesis of Triangular Gold Nanoprisms. *Nat. Mater.* **2004**, *3*, 482−8.
(23) Nune, S. K.; Chanda, N.; Shukla, R.; Katti, K.; Kulkarni, R. R.; Thilakavathi, S.; Mekapothula, S.; Kannan, R.; Katti, K. V Green Nanotechnology from Tea: Phytochemicals in Tea as Building Blocks for Production of Biocompatible Gold Nanoparticles. *J. Mater. Chem.* **2009**, *19*, 2912−2920.
(24) Shukla, R.; Nune, S. K.; Chanda, N.; Katti, K.; Mekapothula, S.; Kulkarni, R. R.; Welshons, W. V.; Kannan, R.; Katti, K. V Soybeans as a Phytochemical Reservoir for the Production and Stabilization of Biocompatible Gold Nanoparticles. *Small* **2008**, *4*, 1425−36.
(25) Menon, D.; Basanth, A.; Retnakumari, A.; Manzoor, K.; Nair, S. V. Green Synthesis of Biocompatible Gold Nanocrystals with Tunable Surface Plasmon Resonance Using Garlic Phytochemicals. *J. Biomed. Nanotechnol.* **2012**, *8*, 901−911.
(26) Narayanan, S.; Sathy, B. N.; Mony, U.; Koyakutty, M.; Nair, S. V.; Menon, D. Biocompatible Magnetite/gold Nanohybrid Contrast Agents via Green Chemistry for MRI and CT Bioimaging ACS. *ACS Appl. Mater. Interfaces* **2012**, *4*, 251−60.
(27) Shankar, S. S.; Rai, A.; Ahmad, A.; Sastry, M. Controlling the Optical Properties of Lemongrass Extract Synthesized Gold Nanotriangles and Potential Application in Infrared-Absorbing Optical Coatings. *Chem. Mater.* **2005**, *17*, 566−572.
(28) U.S. Department of Agriculture, Agricultural Research Service. 2010. Oxygen Radical Absorbance Capacity (ORAC) of Selected Foods, Release 2. Nutrient Data Laboratory Home Page. http://www.ars.usda.gov/nutrientdata/orac.
(29) Jain, P. K.; El-Sayed, I. H.; El-Sayed, M. A. Au Nanoparticles Target Cancer. *Nano Today* **2007**, *2*, 18−29.
(30) Kelly, K. L.; Coronado, E.; Zhao, L. L.; Schatz, G. C. The Optical Properties of Metal Nanoparticles: The Influence of Size, Shape, and Dielectric Environment. *J. Phys. Chem. B* **2003**, *107*, 668−677.
(31) Huang, X.; El-Sayed, M. A. Gold Nanoparticles: Optical Properties and Implementations in Cancer Diagnosis and Photothermal Therapy. *J. Adv. Res.* **2010**, *1*, 13−28.
(32) Veselá, A.; Barros, A. S.; Synytsya, A.; Delgadillo, I.; Copíková, J.; Coimbra, M. A. Infrared Spectroscopy and Outer Product Analysis for Quantification of Fat, Nitrogen, and Moisture of Cocoa Powder. *Anal. Chim. Acta* **2007**, *601*, 77−86.
(33) Andújar, I.; Recio, M. C.; Giner, R. M.; Ríos, J. L. Cocoa Polyphenols and Their Potential Benefits for Human Health. *Oxid. Med. Cell. Longevity* **2012**, *2012*, 906252.
(34) Loo, C.; Lowery, A.; Halas, N.; West, J.; Drezek, R. Immunotargeted Nanoshells for Integrated Cancer Imaging and Therapy. *Nano Lett.* **2005**, *5*, 709−11.
(35) Kirui, D. K.; Rey, D. A.; Batt, C. A. Gold Hybrid Nanoparticles for Targeted Phototherapy and Cancer Imaging. *Nanotechnology* **2010**, *21*, 105105.
(36) Aydogan, B.; Li, J.; Rajh, T.; Chaudhary, A.; Chmura, S. J.; Pelizzari, C.; Wietholt, C.; Kurtoglu, M.; Redmond, P. AuNP-DG: Deoxyglucose-Labeled Gold Nanoparticles as X-Ray Computed Tomography Contrast Agents for Cancer Imaging. *Mol. Imaging Biol.* **2010**, *12*, 463−7.
(37) Sun, I.-C.; Eun, D.-K.; Na, J. H.; Lee, S.; Kim, I.-J.; Youn, I.-C.; Ko, C.-Y.; Kim, H.-S.; Lim, D.; Choi, K.; Messersmith, P. B.; Park, T. G.; Kim, S. Y.; Kwon, I. C.; Kim, K.; Ahn, C.-H. Heparin-Coated Gold Nanoparticles for Liver-Specific CT Imaging. *Chem.—Eur. J.* **2009**, *15*, 13341−7.
(38) Singh, S.; Pasricha, R.; Bhatta, U. M.; Satyam, P. V.; Sastry, M.; Prasad, B. L. V. Effect of Halogen addition to Monolayer protected Gold nanoparticles. *J. Mater. Chem.* **2007**, *17*, 1614−1619.
(39) Joseph, Y.; Besnard, I.; Rosenberger, M.; Guse, B.; Nothofer, H.; Wessels, J. M.; Wild, U.; Knop-Gericke, A.; Su, D.; Schlögl, R.; Yasuda, A.; Vossmeyer, T. Self-Assembled Gold Nanoparticle/Alkanedithiol Films: Preparation, Electron Microscopy, XPS-Analysis, Charge Transport, and Vapor-Sensing Properties. *J. Phys. Chem. B* **2003**, *107*, 7406−7413.
(40) Sileika, T. S.; Barrett, D. G.; Zhang, R.; Lau, K. H. A.; Messersmith, P. B. Colorless Multifunctional Coatings Inspired by Polyphenols Found in Tea, Chocolate, and Wine. *Angew. Chem., Int. Ed.* **2013**, *52*, 1−6.